Science of the Total Environment 583 (2017) 334–343

Contents lists available at ScienceDirect

Science of the Total Environment

journal homepage: www.elsevier.com/locate/scitotenv

Long-range and regional transported size-resolved atmospheric aerosols during summertime in urban Shanghai

Xiaoxiao Ding, Lingdong Kong *, Chengtian Du, Assiya Zhanzakova, Lin Wang, Hongbo Fu, Jianmin Chen *, Xin Yang, Tiantao Cheng

Institute of Atmospheric Sciences, Shanghai Key Laboratory of Atmospheric Particle Pollution and Prevention, Department of Environmental Science & Engineering, Fudan University, Shanghai 200433, China.

HIGHLIGHTS

- Spatial source distributions of size-resolved particles were studied.
- Potential pollution sources of inorganic and carbonaceous aerosols in $PM_{1.8}$-associated particles were studied.
- Important role of ship emission in the air quality of Shanghai in summer.
- Significant contribution of particulate pollutants from long-range transported air masses to PM levels of Shanghai in summer.

GRAPHICAL ABSTRACT

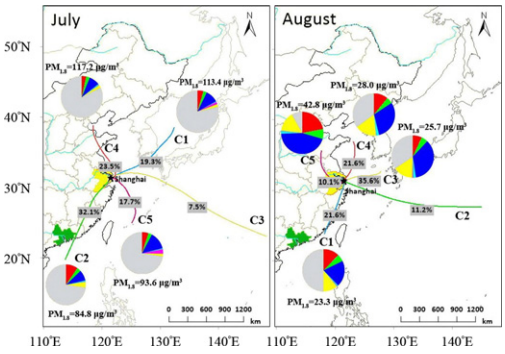

ARTICLE INFO

Article history:
Received 5 December 2016
Received in revised form 11 January 2017
Accepted 11 January 2017
Available online 15 January 2017

Editor: D. Barcelo

Keywords:
Size-resolved aerosol
Regional transport
Long-range transport
PSCF

ABSTRACT

In this study, the concentrations of water soluble ions (WSI), organic carbon (OC), and elemental carbon (EC) of size-resolved (0.056–18 μm) atmospheric aerosols were measured in July and August 2015 in Shanghai, China. Backward trajectory model and potential source contribution function (PSCF) model were used to identify the potential source distributions of size-resolved particles and $PM_{1.8}$-associated atmospheric inorganic and carbonaceous aerosols. The results showed that the average mass concentrations of $PM_{0.1}$, PM_1, and $PM_{1.8}$ were 21.21, 82.90, and 100.1 μg m^{-3} in July and 7.00, 29.21, and 35.10 μg m^{-3} in August, respectively, indicating that the particulate matter pollution was more serious in July than in August in this study due to the strong dependence of the aerosol species on the air mass origins. The trajectory cluster analysis revealed that the air masses originated from heavily industrialized areas including the Pearl River Delta (PRD) region, the Yangtze River Delta (YRD) region and the Beijing-Tianjin region were characterised with high OC and SO_4^{2-} loadings. The results of PSCF showed that the pollution in July was mainly influenced by long-range transport while it was mainly associated to local and intra-regional transport in August. Besides the contributions of anthropogenic sources from YRD and PRD region, ship emissions from the East China Sea also made a great contribution to the high loadings of $PM_{1.8}$ and $PM_{1.8}$-associated NO_3^-, NH_4^+, and EC in July. SO_4^{2-} in Shanghai was dominantly ascribed to anthropogenic sources and the high PSCF values for $PM_{1.8}$-associated SO_4^{2-} observed in August was mainly due to the ship emissions of Shanghai port, such as Wusong port and Yangshan deep-water port. These results indicated that the particulate pollutants from long-range transported air masses and shipping made a significant contribution to Shanghai's air pollution.

* Corresponding author.
E-mail addresses: ldkong@fudan.edu.cn (L. Kong), jmchen@fudan.edu.cn (J. Chen).

http://dx.doi.org/10.1016/j.scitotenv.2017.01.073
0048-9697/

1. Introduction

Located on the eastern tip of the Yangtze River Delta (YRD), e.g. the triangle-shaped territory of Shanghai, southern Jiangsu province, and northern Zhejiang province of China, Shanghai develops with China's largest petrochemical complex, the largest steel plant and many other industries. And it owns the world's busiest container port, whose container throughput totalled 36.5 million TEU (twenty-foot-equivalent units) in 2015. Despite local pollution and intra-regional transport in YRD (Ying et al., 2014), the dust storm from the northwest of China (Wang et al., 2013a) and the polluted air masses from the PRD region, e.g. the dense network of cities that covers nine prefectures of the province of Guangdong and the special administrative regions of Hong Kong and Macau further deteriorates the atmospheric environmental quality of Shanghai. In addition, Shanghai may also under the impact of the vast anthropogenic emissions from East Asian region via long- and medium-range transport due to the monsoon system, which could be associated with the high observed aerosol loadings in Shanghai. Long range transport should contribute a lot to the increase of particulate matter (PM) concentrations in Shanghai.

The PM pollution in Shanghai has drawn increasingly attention in recent years due to its impacts on visibility degradation (Song et al., 2003), climate change (Cifuentes et al., 2001; Forster and Taylor, 2006) and human health (Bell et al., 2006; Iii et al., 2002; Sheppard et al., 1999). The visibility degradation due to PM is generally related to scattering by sulfate, nitrate, ammonium, and certain organic carbon (OC) as well as absorption by elemental carbon (EC) and some other OC (Andreae et al., 2008; Laskin et al., 2010; Sun et al., 2005).

Studies dealt with local pollution sources and long-range transport of the above mentioned aerosol species has been reported during the recent years (Wang et al., 2013a; Zhao et al., 2015). And there are a few studies using a variety of receptor model to determine the sources of aerosols and estimate their contributions to aerosol concentration at receptor site and downwind areas in East Asia (Han et al., 2005; Huang et al., 2007; Jeong et al., 2011; Mochida et al., 2003). However, few study on the characteristics of the long-range transported size-resolved atmospheric inorganic and carbonaceous aerosols in urban Shanghai have been reported. Besides, many studies just take one month of summer as a representative to demonstrate the characteristics of the atmospheric pollution of summer, which has some limitations because great changes could take place due to the differences of the dominant air mass origins among the months even though they all belong to summer.

Therefore, in this study, the concentration of PM in the size range of 0.056–18 μm and its compositions including water soluble ions (F^-, Cl^-, SO_4^{2-}, NO_3^-, Li^+, Na^+, NH_4^+, K^+, Ca^{2+}, Mg^{2+}, formate, acetate, methanesulfonic acid, oxalate) as well as carbonaceous species (OC, EC, SOC) were measured in Shanghai in two typical months (July and August) in summer and the spatial distributions of apportioned anthropogenic sources were analysed by PSCF model. The purposes of the study are 1) to provide the levels of size-resolved PM and its compositions in the urban areas of Shanghai; 2) to learn the contributing sources of size-resolved atmospheric inorganic and carbonaceous aerosols; 3) to get a better understanding of the role of the air mass parcels in facilitating long range transport to the receptor site.

2. Methods

2.1. Particle sampling

Size-segregated aerosol particle samples were collected on the roof (~15 m) of 4th Teaching Building in Fudan University (31.30°N, 121.50°E), Shanghai, China (Fig. 1). The sampling site was under the impact of residential, traffic, industrial and construction emissions, and it was located approximately 90 km to Yangshan Port, one of the largest container ship ports in the world.

Sampling was conducted in July and August, two representative months in the summer of 2015. Sampling of size-segregated aerosol particles was performed on 47 mm quartz filter membranes (PALLFLEX, USA) using the Micro-Orifice Uniform Deposit Impactor (MOUDI) Sampler (MODEL 110-R, MSP CORP., USA), a ten-stage cascade impactor with 50% cut-offs ranging from 0.056 to 18 μm at a flow rate of 30 L min^{-1}. The nominal cut-offs being 18, 10, 5.6, 3.2, 1.8, 1.0, 0.56, 0.32, 0.18, 0.10, 0.056 μm in aerodynamic diameters respectively. Here the inclusion of inlet and backup stages allowed collection of particles in 12 size fractions between <0.056 and >18 μm. One additional backup filter was applied. Prior to use, the quartz membranes were pre-heated at 500 °C for 4 h in a muffle furnace to remove original organic traces. Samples were put in membrane filters boxes right after sampling and reserved in a refrigerator at −18 °C until analysis. The sampling period was 24 h and the sampling work was taken only when the meteorological conditions was favorable (i.e. no wet precipitation and a constant air mass origin throughout the sampling day). 168 and 264 size-segregated aerosol samples were collected in July and August, respectively. All the procedures were strictly quality controlled to avoid any possible contamination of the samples. It should be noted that the experimental study was interrupted on 4–11, 22–26 July due to typhoon "Chanhom" and "Linfa" while 6–11, 20–25 August was under the impact of typhoon "Soudelor" and "Goni", respectively.

The determination of the collected particle mass was done gravimetrically using an intelligent weighing system (Hangzhou Wmade Intelligent Technology co., LTD, reading precision 10 μg) after at least 24 h of equilibration at (20 ± 1) °C with a relative humidity of (40 ± 1) %. After weighing, the quartz filter membranes were cut with ceramic scissors and chemically analysed.

2.2. Chemical analysis

OC and EC in particles were determined by Thermal/Optical Carbon Analyzer (Desert Research Institute (DRI) Model 2001, Atmoslytic Inc., Calabasas, CA, USA). A 0.506 cm^2 punch of each sample was analysed for eight carbon fractions following the IMPROVE TOR protocol. Four OC fractions (OC1, OC2, OC3, and OC4 at 120 °C, 250 °C, 450 °C, and 550 °C, respectively, in a helium atmosphere), and three EC fractions (EC1, EC2, and EC3 at 550 °C, 700 °C, and 800 °C, respectively, in a 2% oxygen/98% helium atmosphere) were produced. During volatilization of organic carbon, part of organic carbon was converted pyrolytically to EC, this fraction of pyrolized organic carbon (PC) is determined by transmittance. A He–Ne laser was employed to monitor the sample reflectance. As pyrolysis occurs, the reflectance decreases. Then, as EC is removed from the filter, the reflectance will increase until all carbon is removed from the filter. IMPROVE OC is operationally defined as OC1 + OC2 + OC3 + OC4 + PC and EC is defined as EC1 + EC2 + EC3 − PC. The concentrations of OC and EC reported here are all corrected for the field blanks. SOC was estimated by EC-based method (Turpin and Huntzicker, 1995) in this study, the primary OC/EC ratio used in the equation was replaced by observed minimum ratio of OC/EC which has been discussed in detail by Castro et al. (1999) and the estimation equation could be written as

$$OC_{sec} = OC_{tot} - EC \times (OC/EC)_{min} \quad (1)$$

For ion analysis, one fourth of each aerosol sample and the blank filter were extracted ultrasonically by 5 mL ultra-pure deionized distilled water (specific resistance ≥18.1 MΩ, Millipore) for 40 min. Water soluble ions F^-, Cl^-, Br^-, SO_4^{2-}, NO_3^-, PO_4^{3-}, Li^+, Na^+, NH_4^+, K^+, Ca^{2+}, and Mg^{2+} as well as formate, acetate, methanesulfonic acid, and oxalate were analysed by an ion chromatography (940 Professional IC, Metrohm, Switzerland.), with an separation columns of Metrosep A supp 16–250, a Metrosep A supp 16 guard column for anion and a Metrosep C6 analytical column, a Metrosep C4 guard column for cation.

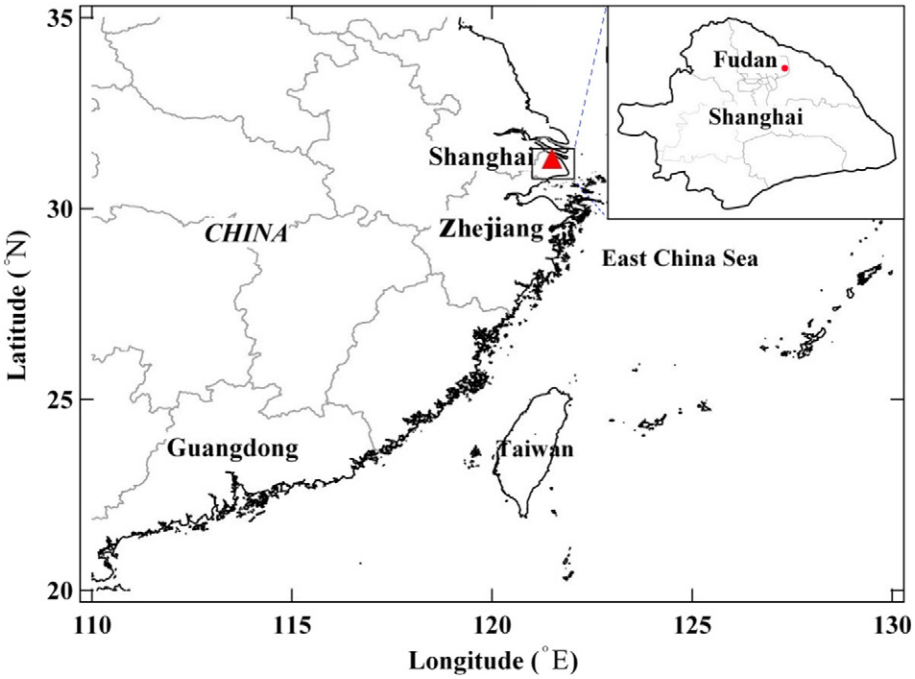

Fig. 1. Location of Fudan site in Shanghai, China.

The relative standard deviation of each ion was <2% from reproducibility tests. Six blank samples were analysed with the same process to remove contamination from blank filters and possible sources of pretreatment.

2.3. Data processing

The cut point of the MOUDI is defined as a diameter with aerosol collection efficiency of 50% (Marple et al., 1991), thus the collected particles in each size bin exhibit an approximately normal distribution against the particle diameter on a logarithmic scale. In this study, the geometric mean value of the two cut-point diameters was used as the average diameter of particles within the size range, and $dC/d\log_{10}Dp$ was calculated to represent the size resolved concentrations in figures with an X axis of particle diameter on a logarithmic scale. To simplify the calculation, the particle modes were divided directly by the cut points in this study. The particle modes were defined as: 0–0.1 μm for nucleation mode, 0.1–0.56 μm for condensation mode, 0.56–1.8 μm for droplet mode, and 1.8–18 μm for coarse mode. Since the cut point of 2.5 μm is not available in this study, the classification of the fine particle pollution conditions in each day was based on $PM_{1.8}$ concentrations.

2.4. Meteorological data and back trajectory analysis

In this study, the meteorological parameters including temperature (T), wind speed (WS) and direction, relative humidity (RH), visibility were routinely measured.

72-h backward trajectories of air masses arriving at the sampling site were calculated using the HYSPLIT model (http://ready.arl.noaa.gov/HYSPLIT.php) to investigate the influence of different air masses from distant sources on aerosol composition. The meteorological data fields used to run the model are available at NOAA's ARL archives. For each sampling day, the model was run with the interval of every hour and the starting height was set as 500 m. The method used in trajectory clustering was based on the GIS-based software TrajStat (http://www.meteothinker.com/TrajStatProduct.aspx) (Wang et al., 2009).

2.5. PSCF models

PSCF model is a method for identifying regional sources based on the HYSPLIT model. The zone of concern is divided into $i \times j$ small equal grid cells. The grid cover area in the range of 10–50° N and 100–160° E was defined, and grid cells of 0.2° × 0.2° were contained in this study.

PSCF is a function of location as defined by the cell indices i and j. The number of endpoints that fall in the ijth cell is designated n_{ij} and the number of endpoints for the same cell having arrival times at the sampling site corresponding to species concentrations higher than an arbitrarily set criterion is defined to be m_{ij}.

In this study, the 25th percentile value of a particular species was treated as the criterion, based on trial and error. The PSCF value for the ijth cell is then defined as

$$PSCF_{ij} = m_{ij}/n_{ij} \quad (2)$$

To reduce the effect of small values of n_{ij}, the PSCF values were multiplied by an arbitrary weight function W_{ij} to better reflect the uncertainty in the values for these cells (Polissar et al., 1998). The weighting function reduced the PSCF values when the total number of the endpoints in a particular cell was less than about three times the average value of the end points per each cell. In this case, W_{ij} was defined as below.

$$W_{ij} = \begin{cases} 1.00 & 80<n_{ij} \\ 0.70 & 20<n_{ij}\le 80 \\ 0.42 & 10<n_{ij}\le 20 \\ 0.05 & n_{ij}\le 10 \end{cases} \quad (3)$$

3. Results and discussion

3.1. Atmospheric concentrations and meteorological conditions

3.1.1. Concentrations of size-resolved PM

The mass concentration of PM_{10} ranged from 26.39 to 194.91 μg m^{-3} with an average of 115.77 μg m^{-3} in this study. Approximately 71% of

the sampling days exceeded the 24-hour PM_{10} standard of 50 μg m^{-3} according to the First Grade National Standard of China and 19% of the sampling days exceeded the Second Grade National Standard (150 μg m^{-3}) (GB3095-2012), indicating the atmospheric PM pollution in Shanghai was very serious. Since July and August are two typical months of summer, the respective performance of these two months have been taken into further discussion.

Table. 1 presented the concentrations of size-resolved PM and the chemical compositions of $PM_{1.8}$ as well as the meteorological conditions in July and August 2015 in Shanghai. As can be seen in Table. 1, the PM_{18} mass concentration of August (62.00 μg m^{-3}) was remarkable lower than that in July (181.07 μg m^{-3}) in this study yet the temperature and RH between these two months did not show an obvious difference. 55% and 57% of the mass concentrations were accounted to fine particles in July and August, respectively, accompanying with 21% and 29% of the mass concentrations accounting to droplet mode in July and August, respectively, indicating the serious fine particle pollution in urban Shanghai. The concentrations of particulate matters followed the sequence of coarse mode > condensation mode > droplet mode > nucleation mode in July, and with the order of coarse mode > droplet mode > condensation mode > nucleation mode in August.

The concentrations of $PM_{0.1}$, PM_1, and $PM_{1.8}$ were 21.21, 82.90, and 100.1 μg m^{-3} in July and 7.00, 29.21, and 35.10 μg m^{-3} in August, respectively. The average concentration of the $PM_{0.1}$ (13.42 μg m^{-3}) for the whole sampling period was much higher than that measured in Taiwan (1.42 μg m^{-3}) (Bamber, 2012). The average concentration of the submicron particles (PM_1) (53.45 μg m^{-3}) for the whole sampling period was much higher than that measured in summer in Guangzhou (Tao et al., 2012) and Jiaxing, Zhejiang (Huang et al., 2013), and the average concentration of PM_1 in July even showed an almost three-fold difference to these researches. Considering that PM_1 should be more closely related with adverse health issues than larger particles (Huang et al., 2003) and the lifetime of smaller size particles can range from days to weeks (Bamber, 2012), the extremely high loadings of $PM_{0.1}$ and PM_1 in Shanghai should attract much attention.

3.1.2. Chemical concentration

Fig. 2 presented the size-resolved aerosol compositions including water soluble ions as well as OC and EC in July and August in this study. It was obvious that the mass concentration in each size range in July was remarkable higher than that in August. However, the measured chemical masses only accounted for 23% of the gravimetric PM_{18} masses in July while the known chemical masses accounted for 68% of the gravimetric PM_{18} masses in August. As for the vast unknown compositions in July which accounted for 77% of PM_{18} masses, would be explained later.

As shown in Fig. 2, particulate matters presented similar two-peak pattern in July and August. One peak was in the fine mode (0.56–1 μm), the other in the coarse mode (5.6–10.0 μm). In this study, the WSI in PM_{18} was 23.44 μg m^{-3} for summer average, with 22.61 μg m^{-3} and 24.12 μg m^{-3} in July and August, respectively, constituting 12% and 39% of the PM_{18} mass concentrations in July and August, respectively. Compared to August, the mass fraction percentage of WSI in July was quite low. Mass fraction percentages of WSI in nucleation mode, condensation mode, droplet mode, and coarse mode were 4%, 12%, 26%, and 8% in July and 17%, 52%, 62%, and 30% in August, respectively. Droplet mode was the most abundant mode for WSI among the four modes in both July and August. For droplet-mode particles, sulfate, nitrate and ammonium (SNA) accounted for 91% and 75% of the WSI in July and August, respectively.

As the most abundant species in WSI, SO_4^{2-} mainly concentrated on the fine particles, especially enriched in droplet mode particles. Nitrate was relatively abundant in coarse mode in both July and August and more nitrate was observed in August (see Fig.2). This can be attributed to the higher temperature in summer, which might make nitrate particles be significantly in the gas phase as nitric acid and thus favor the heterogeneous reactions of nitric acid with coarse mode dust or sea salt particles (Tao et al., 2014). Relatively abundant NH_4^+ was observed in July, especially enriched in droplet and coarse mode particles, while few ammonium was observed in August. This may be explained as the results of the different air mass sources in July and August. Na^+ and Cl^- mainly derived from marine salts. Compared with July, more Na^+ and Cl^- were observed in August, indicating the effect of clean oceanic air on the particles in August. The concentration of Na^+ in August was three folds to that in July. Na^+ accounted for 17% of the WSI in August while the value was 5% in July. The difference was especially obvious in droplet mode, and Na^+ accounted for 19% of the WSI in August while the value was just 2% in July. In coarse mode particles, the molar ratios of Cl^-/Na^+ were 0.95 and 0.33 in July and August, respectively, which may imply more nitrate production and more chlorine depletion in coarse mode in August due to the reaction of gaseous HNO_3 with sea salt. Few water soluble CH_3COO^-, $HCOO^-$, MSA, and $C_2O_4^{2-}$ were observed in this study and more OC and EC were observed in July than in August in PM_{18}.

The concentrations of the WSI in $PM_{1.8}$ were 15.93 μg m^{-3} and 17.62 μg m^{-3}, accounting for 16% and 50% of $PM_{1.8}$ in July and August (Table 1), respectively. The average concentrations of $PM_{1.8}$-associated SO_4^{2-}, NO_3^-, and NH_4^+ were 11.19, 0.71, and 0.84 μg m^{-3} in summer respectively (Table 1). The data of SO_4^{2-} was comparable to those measured in PM_1 (Huang et al., 2013) and in $PM_{2.5}$ (Wang et al., 2016c; Zhao et al., 2015) in the summer of Shanghai, while the $PM_{1.8}$-associated NO_3^- and NH_4^+ were approximately a factor of 6–11 and 3–8 lower than the data reported from these studies. However, the concentrations of $PM_{1.8}$-associated SO_4^{2-}, NO_3^-, and NH_4^+ in July were very close to that reported by Tao et al. (2016), whose sampling site was just the same as ours, showing the influence of geographic position and meteorological conditions on PM composition.

SNA accounted for 82% and 71% of the WSI in $PM_{1.8}$ in July and August, respectively. The ion mass concentrations of SNA in $PM_{1.8}$ followed the sequence of $SO_4^{2-} > NH_4^+ > NO_3^-$ in July, which was the same as that in Hong Kong (Li et al., 2015), while it followed a different order of $SO_4^{2-} > NO_3^- > NH_4^+$ in August, which was the same as many cities in YRD region, such as Jiaxing, Zhejiang (Huang et al., 2013) and Nanjing, Jiangsu (Wang et al., 2016b), revealing the different sources of these constituents in aerosols in July and August. SO_4^{2-} was the most abundant species in SNA, accounting for 81% and 94% of SNA in July and August, respectively, due to the fact that coal is still the major fuel consumption source in China (Zhang et al., 2007). The NH_4^+ which mainly originated from human and animal excrements, and industrial and agriculture activities,

Table 1
Statistics data of size-resolved PM in July and August.

Months	July	August	average
$PM_{0.1}$ (μg m^{-3})	21.21	7.00	13.42
PM_1 (μg m^{-3})	82.90	29.20	53.45
$PM_{1.8}$ (μg m^{-3})	100.10	35.10	64.46
PM_{10} (μg m^{-3})	151.04	53.66	97.64
PM_{18} (μg m^{-3})	181.07	62.00	115.77
Nucleation mode/PM_{18}	12%	11%	12%
Condensation mode/PM_{18}	23%	16%	21%
Droplet mode/PM_{18}	21%	29%	23%
Coarse mode/PM_{18}	45%	43%	44%
$PM_{1.8}$-TWSI	15.93	17.62	16.83
$PM_{1.8}$-SNA	13.06	12.44	12.73
$PM_{1.8}$-SO_4^{2-}	10.61	11.69	11.19
$PM_{1.8}$-NO_3^-	0.79	0.64	0.71
$PM_{1.8}$-NH_4^+	1.67	0.11	0.84
$PM_{1.8}$-OC (μg m^{-3})	6.15	4.51	5.60
$PM_{1.8}$-EC (μg m^{-3})	2.93	1.98	2.61
$PM_{1.8}$-SOC (μg m^{-3})	2.75	2.11	2.54
$PM_{1.8}$-OC/EC	2.10	2.28	2.14
$PM_{1.8}$-SOC/OC	0.45	0.47	0.45
RH (%)	68.95	69.51	69.25
Temperature (°C)	28.45	28.03	28.22
Wind speed (km/h)	19.77	20.47	20.15

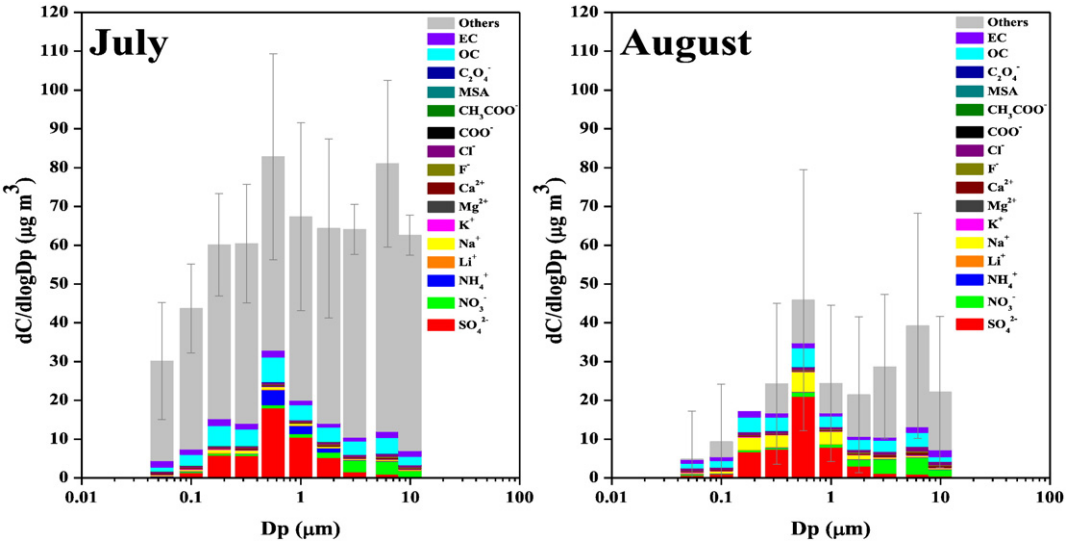

Fig. 2. Size-resolved aerosol compositions in July and August, 2015 in Shanghai. The marker shows the average mass concentration in each size bin with the error bar representing the standard deviation.

accounted for 13% of the SNA in July and 1% of the SNA in August. The possible reasons for the huge difference between two months would be discussed later.

3.1.3. OC and EC

As shown in Table 1, the $PM_{1.8}$-associated TC (sum of OC and EC) concentrations were 9.08 and 6.49 μg m^{-3}, accounting for 9% and 19% of $PM_{1.8}$ in July and August, respectively. For $PM_{1.8}$-associated SOC, it accounted for 45% and 47% of the OC in July and August, respectively, with daily concentrations of 2.75 and 2.11 μg m^{-3} in July and August, respectively. The data of OC, EC and SOC in July were comparable to those measured in $PM_{2.5}$ (Feng et al., 2013; Zhao et al., 2015) in the summer of Shanghai, while the data were a little lower in August.

As reported by previous study, the OC/EC ratios were 1.1 for motor vehicles (Watson et al., 2001), 2.0 for fossil fuel combustion (Cao et al., 2006), and 9.0 for biomass burning (Cachier et al., 1989). The OC/EC ratios for this study exceeded 2.0 for both July and August (Table.1), reflecting the combined contributions from fossil fuel combustion, motor-vehicle exhaust and biomass burning sources.

3.2. Back trajectory cluster analysis

Atmospheric trajectories have been used extensively in studies relating to possible flow paths, source regions, and relevant atmospheric physical/chemical processes. To identify the sources and processes of aerosols in Shanghai atmospheres, backward trajectories of 72-h air masses were investigated during the field campaign. For each day, 24 trajectories were employed with the interval of every hour. The trajectories were mainly grouped into five clusters by clustering algorithm. The five clustering pathways in two months and the mean concentrations of $PM_{1.8}$, OC, EC, and SNA for all trajectory clusters arriving at Shanghai were shown in Fig. 3. The clustering results including mass concentrations as well as the fractions of species for each trajectory cluster were significantly different in July and August as shown in Fig. 3, indicating the strong dependence of the aerosol species on the air mass origins.

The potential pollution sources shown by trajectory clusters were different in July and August. The numbers of the air masses originated from northern China and passed by Shandong Peninsula reached to 23.5% in July (Cluster 4, C4), 2.3 times higher than that in August. The air masses not only carried considerable amount of mineral aerosols from northern China (Wang et al., 2013b), but also contained lots of anthropogenic pollutants due to the industrial activities in Beijing-Tianjin-Hebei region in northern China (Sun et al., 2005; Sun et al., 2015). The abundant concentrations of mineral aerosols as well as the anthropogenic pollutants could elevate the PM concentration significantly over a short period of time (Wang et al., 2013a), which may explain the characteristics of the abundant unknown components in July. The unknown components in July may consist of a lot of water-insoluble minerals and anthropogenic components such as Al, Si, Ca (Wang et al., 2013a) and metallic or non-metallic such as Zn, Cu, Cr, and As (Sharma et al., 2015).

Cluster 1(C1), Cluster 2(C2), and C4 were regarded as polluted and accounted for 75% in July while Cluster 3(C3) and Cluster 5(C5) in July were regarded as relatively clean and accounted for 25%. The statistical results of polluted mean values of $PM_{1.8}$ and $PM_{1.8}$-associated species of each cluster arriving at Shanghai in July were summarized in Table 2. The average $PM_{1.8}$ concentrations associated with polluted trajectories of C1 and C4 were 113.4 μg m^{-3} and 117.2 μg m^{-3}, respectively, higher than the mean value in July, indicating that C1 and C4 had much impact on $PM_{1.8}$ concentrations in Shanghai. C1 and C4 were associated with slower air mass trajectories than other clusters, suggesting that the pollutants emitted from local sources and specific meteorological parameters such as lower wind speed were likely to relate to $PM_{1.8}$ accumulation in July. C1 and C4 also displayed higher polluted mean values of SO_4^{2-}, NO_3^- and NH_4^+, indicating the secondary sources which could originate from local areas as well as from some inland cities via long-range transport. As shown in Table 2, the mentioned relatively abundant NH_4^+ observed in July was mainly derived from C1 and C4, between which C4 was the predominant source. C1 was a long-range trajectory which may be influenced by the East Japan Sea and some Asian countries such as Japan and Korea. C4 was mainly from the north or northeast of China, air masses from this cluster could bring considerable amounts of mineral aerosols and anthropogenic pollutants (Wang et al., 2013b). C2 represented the sources from southern China and passed through the PRD region, where the anthropogenic pollution was also heavy due to the rapid development there (Tao et al., 2012). C2 had the highest OC, EC and SOC loadings among the five clusters and the OC/EC ratio for C2 was also the highest (2.9), indicating the formation of SOA during the transport processes (Zhao et al., 2015), since the ratio of OC/EC exceeding 2.0 usually indicates the presence of SOA (Chow et al., 1996). Potential sources from the areas along this trajectory cluster may have a great contribution to the Shanghai's high OC, EC and SOC concentrations during the observation period. C3 and C5 both represented the marine source. Different from C5, C3 was composed of fast-moving and long trajectories originating from marine which was least influenced while the air masses from C5 may be influenced

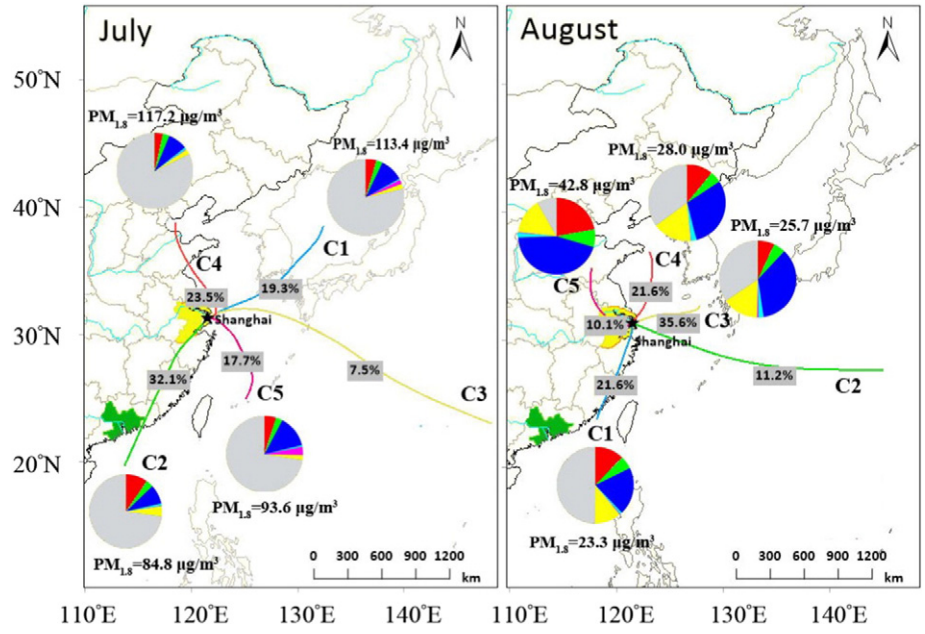

Fig. 3. Mean back trajectories for 5 trajectory clusters arriving at Shanghai in July and August, 2015, with the average fractions of OC, EC, SO_4^{2-}, NO_3^-, NH_4^+ and other water soluble ions in different clusters. The slices are: Red = OC; Green = EC; Blue = SO_4^{2-}; Light blue = NO_3^-; Pink = NH_4^+; Yellow = WSI exclude SNA; Grey = Unknown components. Bright yellow filled region refers to the Yangtze River Delta and Bright green filled region refers to the Pearl River Delta.

by Shanghai Port. As the world's largest port for containers, the problem of vessel emission pollution is quite serious in Shanghai and the ship emissions of Shanghai Port can be considered as one of the major sources of the air pollution in Shanghai (Yang et al., 2007).

Compared with July, August was mainly influenced by short-range transport. C1, C4 and C5 were regarded as polluted and accounted for 32% in August while C2 and C3 in August were regarded as clean and accounted for 68%. The pathway represented by C1 (22%) was most polluted with $PM_{1.8}$ (54.7 μg m^{-3}) while C5 (10%) was most polluted by OC, EC and SOC and also displayed the highest loading of SNA among the clusters. C1 represented the sources from inland, especially from the cities around the PRD. The high SOC/OC ratio of C1 in August (60%) (Table 2), which was the same as that of C2 in July, was very close to that observed in Guangzhou (Fan et al., 2016), which implied the sources of the air masses of these two clusters, indicating the important contributions of emissions from PRD and the areas along the two clusters to the SOA generation in Shanghai. C4 was a short-range trajectory which may be influenced by Northern Yellow Sea, which was heavily polluted by high industrial emissions (Wang et al., 2013b). With the slowest air mass trajectories originated from southwest of Shandong Province, C5 had the least unknown fractions (8%) due to the relatively steady meteorological condition which may favor the accumulation of locally emitted air pollutants via short-range transport. 45% of $PM_{1.8}$ mass was sulfate in this cluster and the high fraction may due to the anthropogenic sources from the industries in local Shanghai and the nearby cities. Also, the high OC/EC ratio (2.9) and SOC/OC (50%) observed in this cluster indicated the significant contribution of anthropogenic pollutants to SOA formation. C2 presented long range transport over the ocean and was quite clean. The numbers of trajectories assigned to C3 were the largest (36%) and the air masses associated with this cluster led to low $PM_{1.8}$ loading (34.3 μg m^{-3}). However, most trajectories were slow-moving and 35% of $PM_{1.8}$ mass was sulfate in C3, suggesting that marine air masses can still transport considerable amounts of sulfate to the sampling site, presumably due to the ship emissions from the nearby ports. C3 had high loading of $PM_{1.8}$-associated WSI and held the highest loading of $PM_{1.8}$-associated NO_3^- while few OC or EC was associated with this cluster.

In addition, the fractions of particulate matters with different size modes were also presented in Table 2. For both July and August, fine particles were the dominant part of the particles, contributed 50%-65% of the atmospheric aerosols. Though the fraction of the nucleation mode was small in both July and August, the value in July was a little higher than that in August. The fractions of different size mode particles for each cluster were similar in July, while the distributions between

Table 2
The statistical results of fraction of particulate matters with different size modes, polluted mean values (μg m^{-3}) of $PM_{1.8}$ and $PM_{1.8}$-associated SO_4^{2-}, NO_3^-, NH_4^+, OC, EC and SOC as well as ratios of OC/EC and SOC/OC of each cluster arriving at Shanghai.

	Cluster	Nucleation mode	Condensation mode	Droplet mode	Coarse mode	$PM_{1.8}$	$PM_{1.8}$							
							SO_4^{2-}	NO_3^-	NH_4^+	OC	EC	SOC	OC/EC	SOC/OC
July	1	7%	29%	29%	35%	113.40	14.20	0.50	2.10	6.80	2.90	2.90	2.30	0.40
	2	5%	31%	24%	39%	84.80	8.40	0.90	0.20	8.20	2.80	4.80	2.90	0.60
	3					0.00	0.00	0.00	0.00	0.00	0.00	0.00		
	4	5%	28%	30%	36%	117.20	15.80	0.80	4.10	5.80	3.40	2.20	1.70	0.40
	5	7%	30%	27%	36%	93.60	8.30	0.80	0.20	3.90	2.70	1.00	1.50	0.30
Aug.	1	3%	22%	37%	38%	54.70	10.10	0.80	0.20	6.90	3.70	3.80	1.80	0.60
	2					0.00	0.00	0.00	0.00	0.00	0.00	0.00		
	3	1%	22%	41%	36%	34.30	11.90	1.50	0.20	0.00	0.00	0.00		
	4	0%	18%	31%	51%	44.00	12.70	1.00	0.10	4.90	3.20	2.00	1.50	0.40
	5	0%	18%	46%	36%	42.80	19.20	1.00	0.20	9.40	3.20	4.60	2.90	0.50

different clusters differed from those in August. The droplet mode contributed considerably in August, which may explain the high fraction of SO_4^{2-} in WSI in August, for SO_4^{2-} was considered being enriched in fine particles, especially being abundant in droplet mode particles as discussed before.

3.3. PSCF

3.3.1. PSCF for size-resolved particles

PSCF provides a more clear visualization of the extent of transport. Fig. 4 presented the weighted PSCF for $PM_{0.1}$, PM_1, $PM_{1.8}$ and PM_{18} in Shanghai during July and August. As shown in Fig. 4, no distinct difference was observed among the distributions of PSCF values for size-resolved PM in July, indicating the similar potential pollution sources for particles with different sizes in July. Potential source areas with weighted PSCF values higher than 0.6 in July were maily located in inland China, include YRD and PRD and the areas that extended from northeast Guangzhou to local Shanghai, indicating the predominant role of anthropogenic sources in PM pollution in urban Shanghai in July, since both YRD and PRD were heavily polluted regions affected by high pollutant emissions due to the rapid economic growth and corresponding rise in energy consumption and vehicle use as well as industrial emissions. Besides, high weighted PSCF values were also seen in July for $PM_{0.1}$, PM_1, $PM_{1.8}$ and PM_{18} in northwest East China Sea (ECS), where there is the Zhoushan Islands, an archipelago in which nineteen-twentieths of the inhabitants are engaged in agriculture. Foreign ships that travel back and forth to the ports there and domestic ship activities between the islands of Zhoushan archipelago both contribute considerably to the ship emissions. According to the results of PSCF, there were also some trails approaching from northern China. The weighted PSCF of size-resolved PM in July indicated that the high particulate pollution of Shanghai in July was mainly ascribed to long-range transport and partly ascribed to regional transport.

Compared with July, the potential source regions of particulate pollution in Shanghai in August were constrained in YRD region. Relatively high weighted PSCF values were presented in local Shanghai, the southern of Jiangsu province, and the northern of Zhejiang province for size-resolved PM, indicating that the particulate pollution of Shanghai in August was mainly ascribed to intra-regional transport in YRD. However, significant differences can be seen among the weighted PSCF for size-resolved particles in August. As shown in Fig. 4(e), the areas of weighted PSCF values higher than 0.6 over the ECS for $PM_{0.1}$ were larger than that for PM_1, $PM_{1.8}$ and PM_{18}, indicating the broader marine sources for $PM_{0.1}$. This result may imply the strong ship primary emissions. It was also clearly shown that besides the YRD region, high PSCF values were also seen in ECS for PM_{18}, indicating the influences of sea salt and ship emissions on the coarse particles (Han et al., 2005; Wang et al., 2016a) observed in August while the submicron and fine particles were mainly related to the anthropogenic emissions from inland China.

3.3.2. PSCF for SNA in $PM_{1.8}$-associated particles

Based on the concentrations of $PM_{1.8}$, $PM_{1.8}$-associated SO_4^{2-}, NO_3^-, and NH_4^+ in Shanghai during July and August, weighted PSCF were plotted in Fig. 5. It was clearly shown that the high fine PM pollution of Shanghai was mainly ascribed to the long-range transport in July while it was mainly ascribed to local and intra-regional transport in August. As shown in Fig. 5, the weighted PSCF results for $PM_{1.8}$-associated NO_3^- and NH_4^+ in July were almost the same as that for $PM_{1.8}$ in the same month, which identified northwest ECS as well as the areas that extended from northeast Guangzhou to local Shanghai as the major potential source regions of $PM_{1.8}$ and $PM_{1.8}$-associated NO_3^- and NH_4^+ in July. Compared to the large scales of potential source regions for $PM_{1.8}$, the areas of high weighted PSCF values(>0.8) for $PM_{1.8}$-associated SO_4^{2-} in July were scattered located at juncture of Jiangxi and Fujian, Zhejiang and Anhui province. These areas were all known to be large emission sources of SO_2.

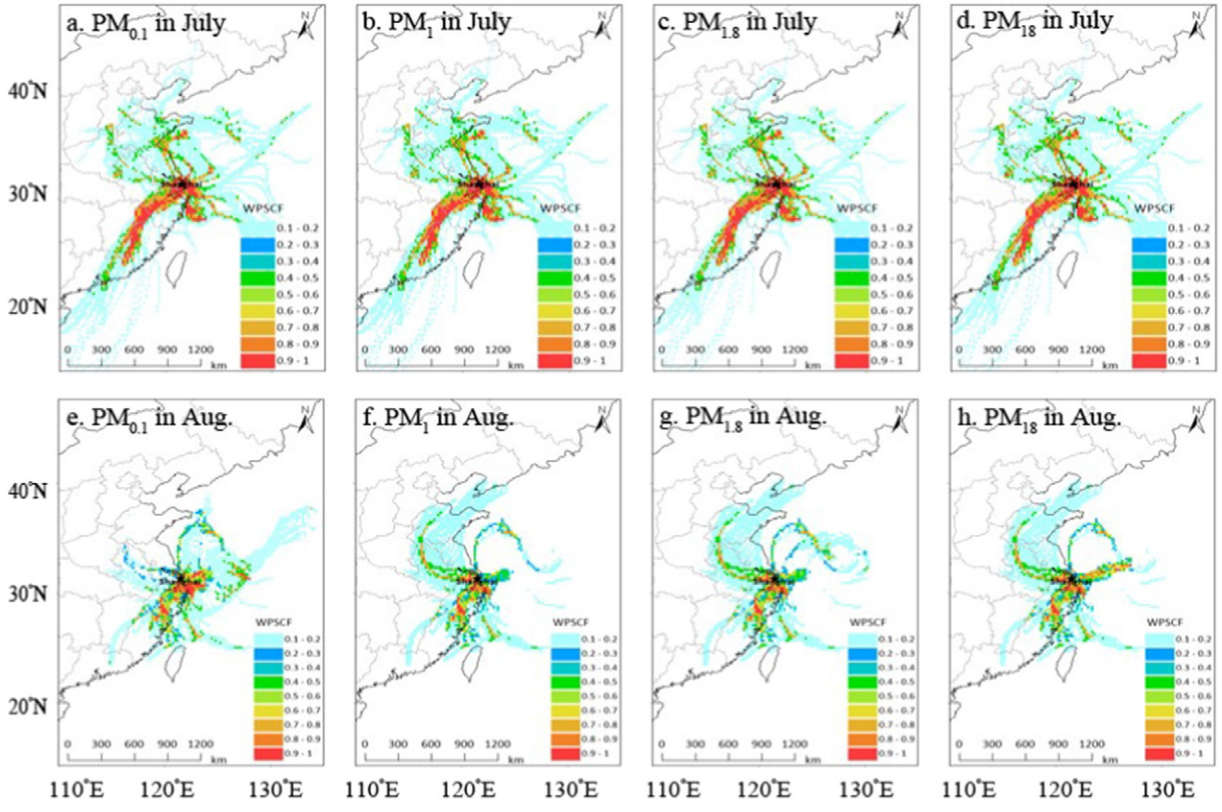

Fig. 4. PSCF for $PM_{0.1}$, PM_1, $PM_{1.8}$ and PM_{18} in July and August.

As for the PSCF for SNA in August, it was worth noting that besides the YRD region, high weighted PSCF values for $PM_{1.8}$-associated SO_4^{2-} were also seen in northwest ECS, where there is Yangshan deep-water Port (Wang et al., 2016a), whose container vessels were required to use marine fuel with sulfur content not exceeding 0.5% when at berth since April 2016, indicating the significant influence of the vessel emissions from the ports on the abundant sulfates observed in the aerosols in Shanghai. Sea-salt (SS) SO_4^{2-} could be estimated based on the assumption that all Na^+ was from the marine source using the marine SO_4^{2-}/Na^+ ratio of 0.25 (Veizer, 1978). It was calculated that SS-SO_4^{2-} accounted for 8% of the total SO_4^{2-} in August and 2% in July, respectively, and these ratios were much higher than those in Haining, Zhejiang (~0.5%) and Zhongshan, Guangdong (~0.8%) (Zhou et al., 2016). This result indicated that SO_4^{2-} in Shanghai was dominantly ascribed to anthropogenic sources yet the contributions of marine sources in August in this study cannot be ignored. The weighted PSCF showed that the $PM_{1.8}$-associated NO_3^- in Shanghai in August was mainly influenced by local sources and the air masses that originated from southwest of Shandong province. As for $PM_{1.8}$-associated NH_4^+, the main potential source region was YRD region, while ECS also contributed much to it in Shanghai in August.

3.3.3. PSCF for carbonaceous aerosols in $PM_{1.8}$-associated particles

Based on the concentrations of $PM_{1.8}$-associated WSI and OC, EC, and SOC in July and August, weighted PSCF were plotted in Fig. 6. The distribution of weighted PSCF values for $PM_{1.8}$-associated WSI was almost the same as $PM_{1.8}$-associated SO_4^{2-}, indicating the dominant role of SO_4^{2-} in WSI. For $PM_{1.8}$-associated OC and EC, the YRD region and the PRD region presented extremely high weighted PSCF values in July, indicating that both long-range transports and regional transports contributed to the carbonaceous pollution in Shanghai in July. Since EC can be transported over long distances due to its light weight and non-volatile characteristics, it can be used as a suitable metric to reflect the influence of long range transported aerosols over a receptor site (Jeong et al., 2011). Besides YRD and PRD, high weighted PSCF values were also seen in ECS for $PM_{1.8}$-associated EC. Since the sampling site in this study is located approximately 90 km to Yangshan Deep-water port, the high weighted PSCF values were evidently due to the contribution from those busy ship activities over the ECS (Wang et al., 2016a).

As shown in Fig. 6(e), the potential source regions of particulate pollution for August were mainly contributed to the local emissions and the impact of ship emissions from Yangshan Port. High weighted PSCF values presented in Yangshan Port for $PM_{1.8}$-associated OC and EC, which was consistent with the results from PSCF analysis of SNA in August, indicated the significant influence of ship emissions on the air quality of Shanghai.

4. Conclusions

Shanghai has frequently suffered from severe particulate matter pollution with the rapid development of economy and urbanization. However, the precise sources of air pollution in Shanghai still remain uncertain. In this study, the concentrations of WSI, OC and EC of size-resolved (0.056–18 μm) atmospheric aerosols were measured in July and August 2015 in Shanghai, China. Backward trajectory model and PSCF model were used to identify the potential source distributions of size-resolved particles and $PM_{1.8}$-associated atmospheric inorganic and carbonaceous aerosols. The results showed that the average mass concentrations of $PM_{0.1}$, PM_1, and $PM_{1.8}$ were 21.21, 82.90, and 100.1 μg m^{-3} in July and 7.00, 29.21, and 35.10 μg m^{-3} in August, respectively, indicating that the particulate matter pollution was more serious in July than in August in this study due to the strong dependence of the aerosol species on the air mass origins. The trajectory cluster analysis revealed that the air masses originated from heavily industrialized areas including the PRD, YRD and the Beijing-Tianjin region were characterised with high OC and SO_4^{2-} loadings. The results of PSCF showed that the pollution in July was mainly influenced by long-range transport while it was mainly associated to local and intra-regional transport in August. The

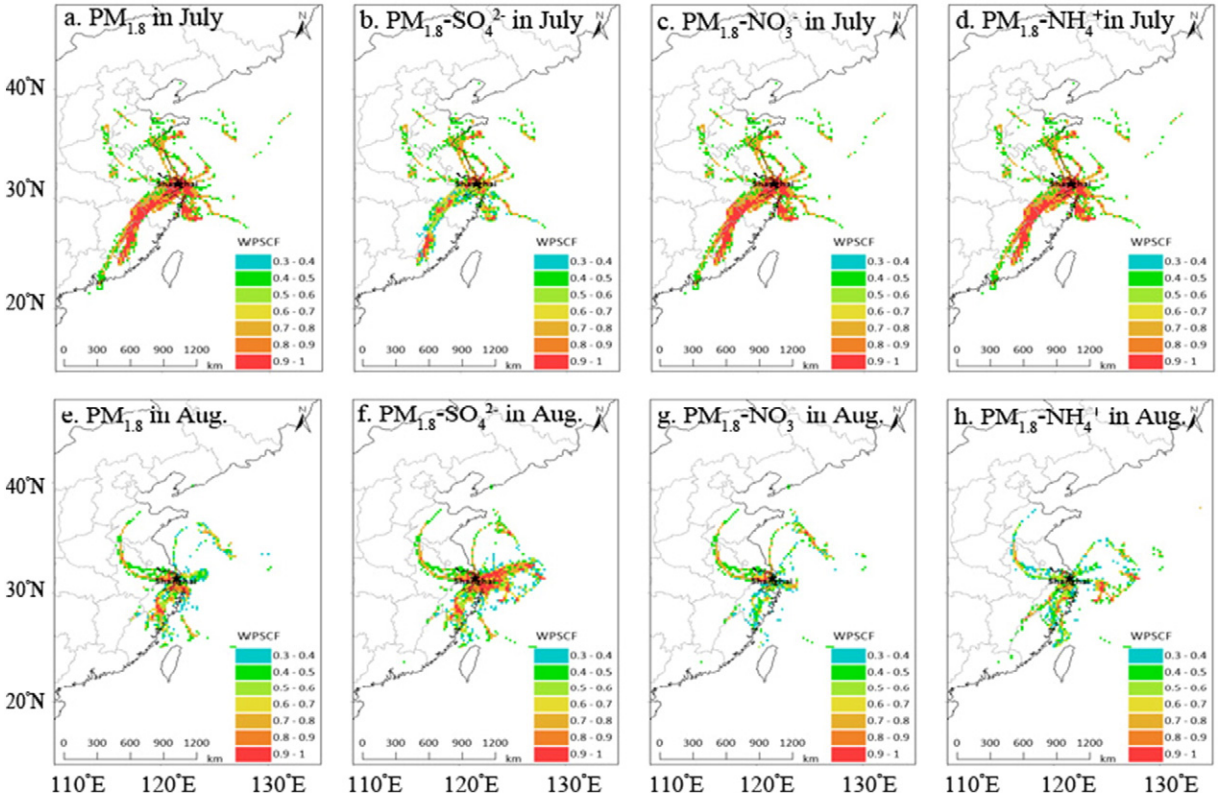

Fig. 5. PSCF for $PM_{1.8}$ and $PM_{1.8}$-associated SNA in July and August.

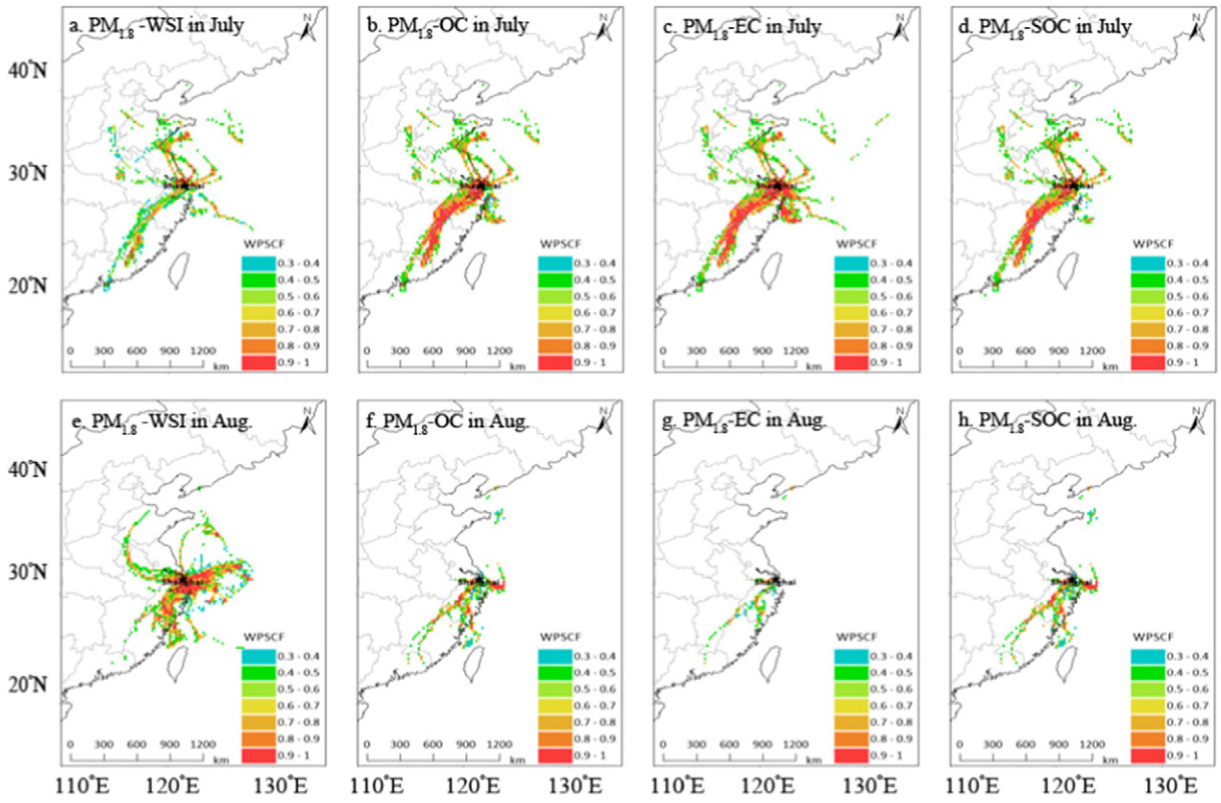

Fig. 6. PSCF for $PM_{1.8}$-associated water soluble ions and OC, EC and SOC in July and August.

potential pollution sources for particles with different sizes in July were similar, while in August the submicron and fine particles were mainly related to the anthropogenic emissions from inland China via local and intra-regional transport yet the coarse particles were also influenced by sea salt and ship emissions. Besides the contributions of anthropogenic sources from the YRD and PRD region, ship emissions from the ECS also made a great contribution to the high loadings of $PM_{1.8}$ and $PM_{1.8}$-associated NO_3^-, NH_4^+, and EC in July. SO_4^{2-} in Shanghai was dominantly ascribed to anthropogenic sources and the high PSCF values for $PM_{1.8}$-associated SO_4^{2-} observed in August was mainly due to the ship emissions of Shanghai port, such as Wusong port and Yangshan deep-water port. These results indicated that the particulate pollutants from long-range transported air masses and shipping made a significant contribution to Shanghai's air pollution. Therefore, it is necessary to implement air pollution control on a larger scale simultaneously, and much attention should be paid to the impact of high potential source from ship emissions on the air quality of Shanghai.

Disclaimer

The authors declare no competing financial interest.

Acknowledgements

This work was supported by the National Natural Science Foundation of China (Grant Nos. 41475110, 21277028, 91544224 and 21190053) and the Key Project of the Shanghai Municipal Science and Technology Commission (Grant No. 14DZ1202903).

References

Andreae, M.O., Schmid, O., Yang, H., Chand, D., Yu, J.Z., Zeng, L.M., et al., 2008. Optical properties and chemical composition of the atmospheric aerosol in urban Guangzhou, China. Atmos. Environ. 42, 6335–6350.

Bamber, G., 2012. Source characterization and apportionment of PM_{10}, $PM_{2.5}$ and $PM_{0.1}$ by using positive matrix factorization. Aerosol Air Qual. Res. 12, 491–496.

Bell, M.L., Davis, D.L., Gouveia, N., Borja-Aburto, V.H., Cifuentes, L.A., 2006. The avoidable health effects of air pollution in three Latin American cities: Santiago, São Paulo, and Mexico City. Environ. Res. 100, 431–440.

Cachier, H., Brémond, M.P., Buatménard, P., 1989. Carbonaceous aerosols from different tropical biomass burning sources. Nature 340, 371–373.

Cao, G., Zhang, X., Zheng, F., 2006. Inventory of black carbon and organic carbon emissions from China. Atmos. Environ. 40, 6516–6527.

Castro, L.M., Pio, C.A., Harrison, R.M., Smith, D.J.T., 1999. Carbonaceous aerosol in urban and rural European atmospheres: estimation of secondary organic carbon concentrations. Atmos. Environ. 33, 2771–2781.

Chow, J.C., Watson, J.G., Lu, Z., Lowenthal, D.H., Frazier, C.A., Solomon, P.A., et al., 1996. Descriptive analysis of $PM_{2.5}$ and PM_{10} at regionally representative locations during SJVAQS/AUSPEX. Atmos. Environ. 30, 2079–2112.

Cifuentes, L., Borja-Aburto, V.H., Gouveia, N., Thurston, G., Davis, D.L., 2001. Assessing the health benefits of urban air pollution reductions associated with climate change mitigation (2000–2020): Santiago, São Paulo, México City, and New York City. Environ. Health Perspect. 109 (Suppl. 3), 419–425.

Feng, J., Li, M., Zhang, P., Gong, S., Zhong, M., Wu, M., et al., 2013. Investigation of the sources and seasonal variations of secondary organic aerosols in $PM_{2.5}$ in Shanghai with organic tracers. Atmos. Environ. 79, 614–622.

Forster, P.M.D.F., Taylor, K.E., 2006. Climate forcings and climate sensitivities diagnosed from coupled climate model integrations. J. Clim. 19, 6181–6193.

Han, J.S., Moon, K.J., Lee, S.J., Kim, Y.J., Ryu, S.Y., Cliff, S.S., et al., 2005. Size-resolved source apportionment of ambient particles by positive matrix factorization at Gosan background site in East Asia. Atmos. Chem. Phys. 5, 5223–5252.

Huang, S.L., Hsu, M.K., Chan, C.C., 2003. Effects of submicrometer particle compositions on cytokine production and lipid peroxidation of human bronchial epithelial cells. Environ. Health Perspect. 111, 478–482.

Huang, Y., Chameides, W.L., Dickinson, R.E., 2007. Direct and indirect effects of anthropogenic aerosols on regional precipitation over east Asia. J. Geophys. Res. Atmos. 112, 855–874.

Huang, X.F., Xue, L., Tian, X.D., Shao, W.W., Sun, T.L., Gong, Z.H., et al., 2013. Highly time-resolved carbonaceous aerosol characterization in Yangtze River Delta of China: composition, mixing state and secondary formation. Atmos. Environ. 64, 200–207.

Iii, C.A.P., Burnett, R.T., Thun, M.J., Calle, E.E., Krewski, D., Ito, K., et al., 2002. Lung cancer, cardiopulmonary mortality, and long-term exposure to fine particulate air pollution. JAMA, J. Am. Med. Assoc. 287, 1132–1141.

Jeong, U., Kim, J., Lee, H., Jung, J., Kim, Y.J., Song, C.H., et al., 2011. Estimation of the contributions of long range transported aerosol in East Asia to carbonaceous aerosol and PM concentrations in Seoul, Korea using highly time resolved measurements: a PSCF model approach. J. Environ. Monit. 13, 1905–1918.

Laskin, J., Laskin, A., Roach, P.J., Slysz, G.W., Anderson, G.A., Nizkorodov, S.A., et al., 2010. High-resolution desorption electrospray ionization mass spectrometry for chemical characterization of organic aerosols. Anal. Chem. 82, 2048–2058.

Li, Y.J., Lee, B.P., Su, L., Fung, J.C.H., Chan, C.K., 2015. Seasonal characteristics of fine particulate matter (PM) based on high-resolution time-of-flight aerosol mass spectrometric (HR-ToF-AMS) measurements at the HKUST Supersite in Hong Kong. Atmos. Chem. Phys. 15, 37–53.

Marple, V.A., Rubow, K.L., Behm, S.M., 1991. A microorifice uniform deposit impactor (MOUDI): description, calibration, and use. Aerosol Sci. Technol. 14, 434–446.

Mochida, M., Kawamura, K., Umemoto, N., Kobayashi, M., Matsunaga, S., Lim, H.J., et al., 2003. Spatial distributions of oxygenated organic compounds (dicarboxylic acids, fatty acids, and levoglucosan) in marine aerosols over the western Pacific and off the coast of East Asia: continental outflow of organic aerosols during the ACE-Asia campaign. J. Geophys. Res. Atmos. 108, 223–224.

Polissar, A.V., Hopke, P.K., Paatero, P., Malm, W.C., Sisler, J.F., 1998. Atmospheric aerosol over Alaska: 2. Elemental composition and sources. J. Geophys. Res. Atmos. 103, 19045–19057.

Sharma, S.K., Sharma, A., Saxena, M., Choudhary, N., Masiwal, R., Mandal, T.K., et al., 2015. Chemical characterization and source apportionment of aerosol at an urban area of Central Delhi, India. Atmos. Pollut. Res. 7, 110–121.

Sheppard, L., Levy, D., Norris, G., Larson, T.V., Koenig, J.Q., 1999. Effects of ambient air pollution on nonelderly asthma hospital admissions in Seattle, Washington, 1987-1994. Epidemiology 10, 23–30.

Song, Y., Tang, X., Fang, C., Zhang, Y., Min, H.U., Zeng, L., et al., 2003. Relationship between the visibility degradation and particle pollution in Beijing. Acta Sci. Circumst. 23, 468–471.

Sun, Y., Zhuang, G., Wang, Y., Zhao, X., Li, J., Wang, Z., et al., 2005. Chemical composition of dust storms in Beijing and implications for the mixing of mineral aerosol with pollution aerosol on the pathway. J. Geophys. Res. Atmos. 110, 1064–1067.

Sun, Y.L., Wang, Z.F., Du, W., Zhang, Q., Wang, Q.Q., Fu, P.Q., et al., 2015. Long-term real-time measurements of aerosol particle composition in Beijing, China: seasonal variations, meteorological effects, and source analysis. Atmos. Chem. Phys. 15, 10149–10165.

Tao, J., Shen, Z., Zhu, C., Yue, J., Cao, J., Liu, S., et al., 2012. Seasonal variations and chemical characteristics of sub-micrometer particles (PM_1) in Guangzhou, China. Atmos. Res. 118, 222–231.

Tao, Y., Yin, Z., Ye, X., Ma, Z., Chen, J., 2014. Size distribution of water-soluble inorganic ions in urban aerosols in Shanghai. Atmos. Pollut. Res. 5, 639–647.

Tao, Y., Ye, X., Jiang, S., Yang, X., Chen, J., Xie, Y., et al., 2016. Effects of amines on particle growth observed in new particle formation events. J. Geophys. Res.-Atmos. 121, 324–335.

Turpin, B.J., Huntzicker, J.J., 1995. Identification of secondary organic aerosol episodes and quantitation of primary and secondary organic aerosol concentrations during SCAQS. Atmos. Environ. 29, 3527–3544.

Veizer, J., 1978. The Chemistry of the Atmosphere and Oceans by Heinrich D. 56. Wiley, Holland, pp. 1117–1118 (6).

Wang, Y.Q., Zhang, X.Y., Draxler, R.R., 2009. TrajStat: GIS-based software that uses various trajectory statistical analysis methods to identify potential sources from long-term air pollution measurement data. Environ. Model. Softw. 24, 938–939.

Wang, L., Du, H., Chen, J., Zhang, M., Huang, X., Tan, H., et al., 2013a. Consecutive transport of anthropogenic air masses and dust storm plume: two case events at shanghai, China. Atmos. Res. 127, 22–33.

Wang, L., Qi, J.H., Shi, J.H., Chen, X.J., Gao, H.W., 2013b. Source apportionment of particulate pollutants in the atmosphere over the Northern Yellow Sea. Atmos. Environ. 70, 425–434.

Wang, F., Chen, Y., Meng, X., Fu, J., Wang, B., 2016a. The contribution of anthropogenic sources to the aerosols over East China Sea. Atmos. Environ. 127, 22–33.

Wang, H., An, J., Cheng, M., Shen, L., Zhu, B., Li, Y., et al., 2016b. One year online measurements of water-soluble ions at the industrially polluted town of Nanjing, China: sources, seasonal and diurnal variations. Chemosphere 148, 526–536.

Wang, H.L., Qiao, L.P., Lou, S.R., Zhou, M., Ding, A.J., Huang, H.Y., et al., 2016c. Chemical composition of $PM_{2.5}$ and meteorological impact among three years in urban Shanghai, China. J. Clean. Prod. 112, 1302–1311.

Watson, J.G., Chow, J.C., Houck, J.E., 2001. $PM_{2.5}$ chemical source profiles for vehicle exhaust, vegetative burning, geological material, and coal burning in Northwestern Colorado during 1995. Chemosphere 43, 1141–1151.

Yang, D.Q., Kwan, S.H., Lu, T., Fu, Q.Y., Cheng, J.M., Streets, D.G., et al., 2007. An emission inventory of marine vessels in Shanghai in 2003. Environ. Sci. Technol. 41, 5183–5190.

Ying, Q., Wu, L., Zhang, H., 2014. Local and inter-regional contributions to $PM_{2.5}$ nitrate and sulfate in China. Atmos. Environ. 94, 582–592.

Zhang, M., Wang, S., Wu, F., Yuan, X., Zhang, Y., 2007. Chemical compositions of wet precipitation and anthropogenic influences at a developing urban site in southeastern China. Atmos. Res. 84, 311–322.

Zhao, M., Huang, Z., Qiao, T., Zhang, Y., Xiu, G., Yu, J., 2015. Chemical characterization, the transport pathways and potential sources of $PM_{2.5}$ in Shanghai: seasonal variations. Atmos. Res. 158, 66–78.

Zhou, J., Xing, Z., Deng, J., Du, K., 2016. Characterizing and sourcing ambient $PM_{2.5}$ over key emission regions in China I: water-soluble ions and carbonaceous fractions. Atmos. Environ. 135, 20–30.